Climate Dynamics (2005) 25: 315–327
DOI 10.1007/s00382-005-0034-3

C. Hatté · J. Guiot

Palaeoprecipitation reconstruction by inverse modelling using the isotopic signal of loess organic matter: application to the Nußloch loess sequence (Rhine Valley, Germany)

Received: 16 June 2004 / Accepted: 25 April 2005

Abstract A modified version of the Biome4 vegetation model for simulation of the mean $\delta^{13}C$ of plant communities is presented, and used to reconstruct palaeoprecipitation. We treat all fractionations by C3 and C4 plants in all coexistent Plant Functional Types, weighted by their respective net primary production. We constrain the range of variation in the intracellular versus atmospheric CO_2 concentration by fixing a lower limit. Finally, we replace some constant parameters by functions of external forcing to account for their responses to environmental variation. The new version of Biome4 was applied as an inverse model and tested on three modern data sets. The fit between observations and simulations is very close to the 1:1 relationship, with respective slopes of 0.90 ± 0.02 ($r^2 = 0.98$, $n = 29$) for $\delta^{13}C$ and 0.97 ± 0.06 ($r^2 = 0.90$, $n = 29$) for precipitation. Inverse modelling was applied using the Metropolis-Hastings algorithm to the Nußloch loess sequence. Over the last glaciation, simulated palaeoprecipitation varies between 240 mm year^{-1} and 400 mm year^{-1}. This study clearly demonstrates atmospheric teleconnections with the Greenland ice-sheet extension, by matching Dansgaard-Oeschger events with precipitation increase of ca. 100–200 mm year^{-1}.

1 Introduction

During the last glaciation, rapid climatic changes occurred on a millennial scale. These changes have been found mainly in marine cores (Bond cycles, Bond et al. 1993) and in ice records (Dansgaard-Oeschger cycles, Dansgaard et al. 1993), as they are difficult to recognise on the continents where the environment has greatly affected human activity. Furthermore, most continental (palaeo)studies focus on temperature (Rousseau 1991; Grimm et al. 1993; Porter and Zhisheng 1995; Guo et al. 1996; Genty et al. 2003). As water availability is one of the major challenges for the future, it is also important to address the hydrological cycle.

Loess deposits are ideal terrestrial archives for the study of palaeoclimate during glacial periods that are otherwise poorly documented in pollen sequences. Contrary to interglacial soils, typical loess accumulates very quickly, recording abrupt climate changes. Moreover, these deposits are associated with sparse vegetation and a weak rhizosphere. As shown by the presence of some laminated structures, these conditions preserve the memory of the contemporaneous climatic conditions at the time of deposit. The absence of pedogenesis, and the dry glacial environment favour the degradation of organic matter without distortion of the isotopic signal, making typical loess suitable for an organic geochemical study. The carbon isotopic composition ($\delta^{13}C$) of loess organic matter nicely reflects the original isotopic signature of vegetation, and therefore acts as an indicator of palaeoenvironmental conditions. In Western Europe, $\delta^{13}C$ ranging from $-23‰$ to $-26‰$ indicates that, during the last climatic cycle, only plants using the C3 photosynthetic pathway existed (Hatté et al. 1998). Thus $\delta^{13}C$ variations were interpreted as changes in environmental conditions related primarily to the concentration and isotopic composition of atmospheric CO_2 as well as water availability and, secondarily, to temperature, soil type and texture, and insolation.

Using a linear relationship between $\delta^{13}C$ and CO_2 concentration and isotopic composition on the one hand and precipitation on the other, Hatté et al. (2001a) at-

C. Hatté (✉)
LSCE, UMR CEA-CNRS 1572, Domaine du CNRS,
91198, Gif-sur-Yvette, France
E-mail: hatte@lsce.cnrs-gif.fr

J. Guiot
CEREGE, UMR 6635 CNRS/Université d'Aix-Marseille III,
Europôle Méditerranéen de l'Arbois, BP 80, 13545,
Aix-en-Provence cedex 4, France

tempted a first deconvolution of the $\delta^{13}C$ record to reconstruct palaeoprecipitation. However, palaeoclimatic inferences were limited, due to the fact that only parameters of the first order were taken into account. The use of vegetation models can introduce a greater complexity by considering first and second order parameters and improve palaeoprecipitation reconstruction. Inverse vegetation modelling has been used previously to reconstruct palaeoclimates from palynological spectra (Guiot et al. 2000) and, recently, from the C4/C3 ratio (Boom et al. 2002). Boom et al. (2002) compared the C4 ratio calculated from isotopic measurements of alkanes with the C4 ratio output from Biome3 for reconstructing past CO_2 concentration. Our objective here is to directly use the isotopic ratios, an output of a vegetation model.

We use Biome4, a modified version of Biome3 (Haxeltine and Prentice 1996), where an isotope subroutine has been incorporated (Kaplan et al. 2002). However, the fit between isotopic fractionation simulations and observations is not sufficiently close to the 1:1 relationship (Fig. 1 for an Australian dataset). We therefore modified the Biome4 model to improve the simulation of the mean $\delta^{13}C$ of plant communities, and tested it against modern data sets. Finally, we inverted the model, applying the Metropolis-Hastings technique to Northwestern Europe by using the loess reference of the Nußloch sequence (Rhine Valley, Germany). The loess series enjoys a high temporal resolution (over 1 m for 1,000 years), supported by a fine and reliable chronology (Hatté et al. 2001b; Lang et al. 2003), and has already been the subject of numerous geochemistry, pedostratigraphy, malacology, and magnetic susceptibility studies (Hatté et al. 1998, 1999, 2001a; Antoine et al. 2001; Moine et al. 2002; Rousseau et al. 2002).

2 Method

2.1 Model Biome4

Biome4 (Kaplan et al. 2002) is a process-based terrestrial biosphere model, modified from Biome3 (Haxeltine and Prentice 1996). Model inputs include data on latitude, soil textural class, and monthly climate (temperature, precipitation and insolation). Incoming solar radiation is calculated considering present-day orbital parameters and a global average albedo. The model usually runs on a 0.5° grid, but can run on any site with complete climatic and soil data. Biome4 considers 13 potential Plant Functional Types (PFTs), representing the major bioclimatic types and growth forms of terrestrial plants. The association of PFTs enables the determination of a single biome amongst 28 potential candidates (Table 1). The Biome4 model includes a photosynthesis scheme that simulates acclimation of plants to external forcing by optimisation of net primary production (NPP) and leaf area index (LAI). Additional rules for approximating the influence of light, canopy, fire risk, and snow are also included. In order to optimise NPP and LAI so as to take external forcing into account, Biome4 uses a coupled carbon and water flux model, to solve a variation in leaf stomatal aperture through iterative calculation, as a response to a moisture-stressed environment. Indeed, in terrestrial vegetation models, this leaf stomatal aperture is usually characterised by the ratio between intracellular and atmospheric CO_2 concentration, C_i/C_a. The iterative calculation starts from a priori C_i/C_a values defined for each PFT and from the photosynthetic pathway. Competition among PFTs is simulated by using the optimal NPP of each PFT as an index of competitiveness. By comparing the optimised NPPs of each PFT,

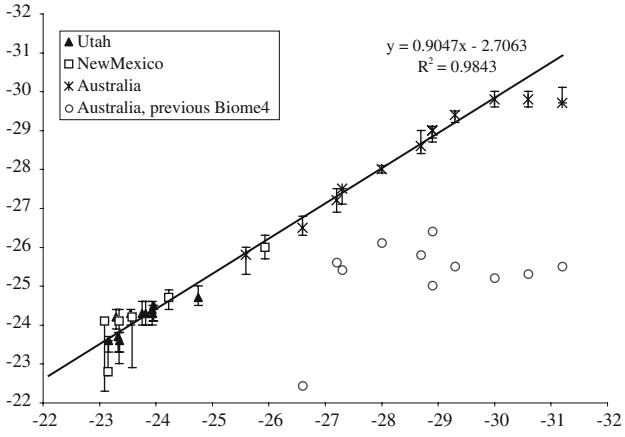

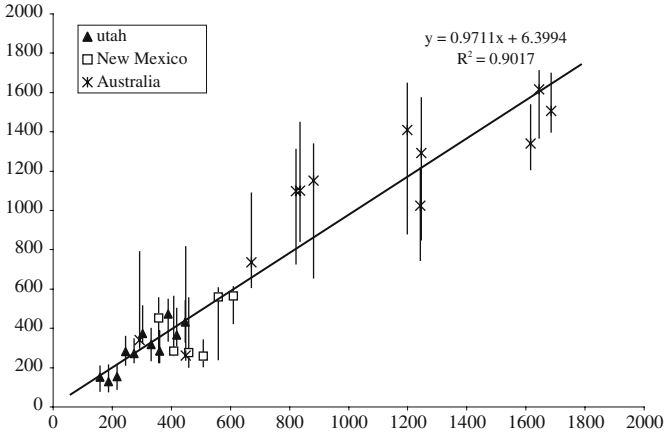

Fig. 1 Modern data sets. The simulation results are presented versus the observed data for $\delta^{13}C$ (*left hand*) and annual precipitation (*right hand*). *Open circles* stand for simulated precipitation obtained for the Australian data set with the original Biome4 version. The simulation results are presented with an error margin; however in order to keep the figures easy to read, no variation range is shown for the observations. Data are compiled in Table 2. The regression lines and their r^2 correlating all observations are shown as well. Notice that, for the range of paleoreconstruction (precipitation lower than 800 mm year^{-1}), the relationship between observed and simulated precipitation displays a slope of 0.95 ± 0.14 ($r^2 = 0.72$, $n = 19$)

Table 1 List of the 28 biomes assigned to Biome4 (biome number, abbreviation and extended name) and corresponding groups of biomes as designed in this study for inverse modelling (group number and name)

List of the 28 biomes			List of the 7 groups of biomes
Biome n°	Abbreviation	Extended name	Group n° group name
1	TrEgFo	Tropical evergreen forest	1 Tropical forest
2	TrSeDeFo	Tropical semi-deciduous forest	1 Tropical forest
3	TrDeFo	Tropical deciduous forest/woodland	1 Tropical forest
4	TeDeFo	Temperate deciduous forest	4 Temperate forest
5	TeCoFo	Temperate conifer forest	4 Temperate forest
6	WaMxFo	Warm mixed forest	4 Temperate forest
7	CoMxFo	Cool mixed forest	4 Temperate forest
8	CoCoFo	Cool conifer forest	4 Temperate forest
9	CIMxFo	Cold mixed forest	5 Boreal forest
10	EgTaig	Evergreen taiga/montane forest	5 Boreal forest
11	DeTaig	Deciduous taiga/montane forest	5 Boreal forest
12	TrSav	Tropical savanna	2 Tropical grassland
13	TrXeShl	Tropical xerophytic shrubland	2 Tropical grassland
14	TeXsShl	Temperate xerophytic shrubland	3 Temperate grassland
15	TeXsWol	Temperate sclerophyll woodland	3 Temperate grassland
16	TeBlSa	Temperate broadleaved savanna	3 Temperate grassland
17	OpCoWol	Open conifer woodland	5 Boreal forest
18	BoPrkl	Boreal parkland	6 Boreal grassland
19	TrGrl	Tropical grassland	2 Tropical grassland
20	TeGrl	Temperate grassland	3 Temperate grassland
21	Desert	Desert	2 Tropical grassland
22	StTund	Steppe tundra	6 Boreal grassland
23	ShTund	Shrub tundra	6 Boreal grassland
24	DShTund	Dwarf shrub tundra	6 Boreal grassland
25	PsShTund	Prostrate shrub tundra	6 Boreal grassland
26	CuTund	Cushion forb lichen moss tundra	6 Boreal grassland
27	Barren	Barren	7 None
28	Lice	Land ice	7 None

Biome4 determines the dominant, co-dominant, and grass-dominant (if different from the two others PFTs). Biome4 then determines the output biome from the successful PFTs, the corresponding NPP, respiration, growth primary production (GPP = NPP-respiration), and LAI. Fractionations by C3 and C4 plants are calculated using the Lloyd and Farquhar (1994) model (mainly using parameters defined during in vitro experiments). The mean annual isotopic fractionation is calculated by weighting monthly fractionation by the respective GPP. Biome4 then attributes to the output biome the isotopic fractionation calculated for the dominant PFT; if the dominant PFT includes C4 and C3 plants, it only considers the dominant photosynthetic type plants. Therefore, it neglects the co-existing PFTs and the sub-dominant photosynthetic type plants.

2.2 Biome4 revisions

We introduced several changes to different parts of the Biome4 program. First, a lower limit of the C_i/C_a ratio was introduced. Secondly, all the isotopic fractionations of both photosynthetic pathways for all coexistent PFTs were taken into account and weighted by NPP. Thirdly, some constant parameters of the Lloyd and Farquhar (1994) model were replaced by functions of environmental parameters.

(a) The optimisation of NPP and LAI by successive iterations of C_i/C_a (necessary to determine the output PFT and biome) may result in a decrease of the C_i/C_a ratio and, since no lower limit is prescribed, may result in a quasi-closing of the stomatal aperture. As it determines internal CO_2 partial pressure, C_i/C_a has a major impact on total fractionation of ^{13}C: the more the stomata are closed, the lower is the exchange between intracellular spaces and the atmosphere. Consequently, the assimilation of heavy carbon increases and $\delta^{13}C$ goes up. Thus, because Biome4 sets no lower limit, a C3 plant could appear as having a C4 signal, with a high $\delta^{13}C$. Farquhar et al. (1982) determined a ratio ranging from 0.95 to 0.36, with a mean at around 0.63. Wong et al. (1979) reported a mean ratio of 0.7. Constable and Rawson (1980) measured values in the 0.48–0.76 range, and Sharkey and Raschke (1981) presented higher values ranging from 0.87 to 0.98. We define a lower limit for C_i/C_a of C3 plants at 0.5, close to the lowest values measured experimentally.

(b) Whereas the original Biome4 only accounts for the dominant photosynthetic pathway in the dominant PFT, our modification accounts for both photosynthetic pathways co-existing in all potential PFTs. Thus a new matrix is introduced, including each intermediate value of NPP, GPP, and isotopic fractionations for C3, and C4 plants if they exist.

Furthermore, in contrast to the original Biome4 version, we adopted the approach, also followed by Scholze et al. (2003), of weighting various intermediate fractionations by the respective NPP instead of GPP. This weighting defines the isotopic fractionation of stored carbon rather than the total carbon that entered the leaves.

(c) The routine calculating the isotopic fractionation of C3 plants is based upon the Lloyd and Farquhar (1994) model. The published parameters in this model mainly result from in vitro experiments under fixed optimal current conditions, i.e. 20 or 25°C, ≈350 ppmv CO_2, and with no nutrient or water limitations. The discrimination against $^{13}CO_2$ during photosynthetic fixation of CO_2 (coefficient b in Lloyd and Farquhar's model) was established at 25°C and varied between 26.4‰ and 28.2‰. An average value of 27.5‰ was selected, but is valid only at 25°C. The revised version of Biome4 considers the isotopic fractionation due to photosynthetic fixation of CO_2 as temperature-dependent. In standard air (i.e. 350 ppmv CO_2, 25°C, and 21% O_2), the influence of photorespiration is small and is assumed to be close to zero. Nevertheless, the intrinsic discrimination of photorespiratory decarboxylation of glycine (coefficient f in the Lloyd and Farquhar (1994) model) depends on the partial pressure of CO_2 in the external atmosphere and intracellular spaces, and consequently is dependent on the CO_2 concentration. From different environmental studies, a negative relationship between CO_2 concentration and $\delta^{13}C$ in plants has been determined (Krishnamurthy and Epstein 1990; Van de Water et al. 1994; Feng and Epstein 1995; Pasquier-Cardin et al. 1999). All of these studies agree with the one published by Feng and Epstein (1995) yielding a $\delta^{13}C$ decrease of 2.0 ± 0.1‰ for an increase in atmospheric CO_2 of 100 ppmv. Therefore, rather than using a constant value off (equal to eight in the original Biome4), we introduce a CO_2 concentration-dependent factor, adjusted to best simulate the relationship between CO_2 concentration and isotopic fractionation. Finally, the contribution of dark respiration to discrimination has also been extensively studied (Park and Epstein 1961; Hsu and Smith 1972; Troughton et al. 1974; Francey et al. 1985; Lin and Ehleringer 1997; Duranceau et al. 1999). This term is normally considered to have only a weak impact on total fractionation, even if its exact extent is not known. Several values are available in the literature, varying from 6‰ to −4‰, and we chose 0.1‰.

2.3 Inverse modelling

We use here the revised version of the process-based vegetation model Biome4 in an inverse mode (i.e. starting from the outputs to infer some of the inputs of the model) to reconstruct the most probable climate. We follow the procedure of Guiot et al. (2000), based on a Monte-Carlo sampling of monthly precipitation and monthly temperature in a pre-defined range (Metropolis-Hastings algorithm, Hastings 1970).

The output biome and the plant NPP are constrained as much by temperature (annual distribution and absolute value) as by precipitation. The carbon isotopic composition is highly dependent on precipitation. Therefore, adding $\delta^{13}C$, to the output biome, as a constraining parameter for the inversion procedure narrows the range in precipitation variation and, as a result better constrains the temperature range as well. The bioindicator loess records do not precisely define the biome that is contemporaneous with the deposit. Pollen grains are too sparse to permit a palynological study, but the range of possible biomes may be deduced from pedology and malacology (molluscs). We consequently regroup the 28 potential biomes into seven biome groups: tropical forest, tropical grassland, temperate grassland, temperate forest, boreal forest, boreal grassland, and "none" (barren and ice land) (Table 1).

In the inverse modelling process, some inputs are known and some are not. First, the known inputs characterise the site and/or the age-dependent parameters (i.e. soil type and texture, altitude, atmospheric CO_2 concentration and isotopic value). Second, the unknown inputs, regarded as constraints for the inverse modelling towards which the simulation must tend, are the average $\delta^{13}C$ observed and one or two pre-defined groups of biomes out of the seven defined above. The agreement between the modelled outputs and the set of observations is evaluated by a numerical distance that takes into account the isotopic value and occurrence of the simulated biome in the predefined groups of biomes:

$$D^2 = -\frac{5 \min\left[(b_1 - b_s)^2, (b_2 - b_s)^2\right] + (\delta^{13}C_o - \delta^{13}C_s)^4}{S^2}$$

where b_1, b_2, and b_s are, respectively, the observed biome (first and second choice) and the simulated biome, the subscripts o and s for $\delta^{13}C$ correspond to observed and simulated values, and S^2 is the inverse of the residual variance, also called the precision of the estimates. b is the biome group number from one to seven. We allow the algorithm to choose between two groups of input biomes so as to enhance its flexibility (first (1) and second (2) choice). The factor five is used so that the order of magnitude of biome number is comparable to that of the $\delta^{13}C$, while the exponent four for $\delta^{13}C$ is used to give more weight to a discrepancy in $\delta^{13}C$ than in the biome number. We exploit five parameters to maximise D^2 : (a) January temperature, (b) July temperature, (c) January precipitation, (d) July precipitation, and (e) S^2 the model precision. The last parameter represents the inverse of the fitting error, and is also an adjustable parameter related to the units of the $\delta^{13}C$ variable. The above equation is calibrated to vary between 0 and 10; a perfect fit having a

precision of 10. The temperature and precipitation of the other months are calculated by sinusoidal interpolation between January and July. Sunshine percentage is also an input of Biome4, and is estimated by linear regression from temperature and precipitation of the same month, as described by Guiot et al. (2000).

The inversion process starts with random values for the five parameters taken from initial sampling intervals. Those parameters are defined as anomalies from a reference state. The required climatic variables (i.e. monthly precipitation, temperature, and cloudiness) are also calculated as anomalies. The five input parameters are updated to new values according to the rules of the algorithm, and a new run is performed. The probability distribution of the five input parameters is computed after several thousand iterations, while that of $\delta^{13}C$ is also calculated, and compared with the observed value as a quality-check for the fit. All distributions are calculated within the 95%-confidence range.

2.4 Modern data

To our knowledge, only two studies available in literature are sufficiently detailed to validate our revised model under modern and natural conditions. One follows transect along Australia, covering a wide range of precipitation and landscapes (Stewart et al. 1995). The other presents leaf $\delta^{13}C$ variability in the southwestern United States (Van de Water et al. 2002).

2.4.1 Australia

Stewart et al. (1995) analysed 12 plant communities along a 900 km-long rainfall gradient in southern Queensland (Australia), which accounts for annual precipitation from 290 mm year^{-1} up to 1690 mm year^{-1}. In order to closely approximate the great diversity in taxonomy, a mean of 29 species was sampled for each site. The community-averaged $\delta^{13}C$ signature ranged from $-25.6‰$ in a brigalow-dominated community in western Queensland to $-31.2‰$ in a subtropical rainforest in eastern Queensland. Simulations based on five different couples of biome categories were performed to reproduce the diversity of landscapes, mostly based either on tropical biomes (forest and/or grassland) or with an opening in the temperate forest, to allow for the simulation of "dry rainforest" and "open forest" (Table 2).

2.4.2 United States

Samples were taken from deserts and woodlands along two transects in southeastern Utah and south central New Mexico (Van de Water et al. 2002). Climatic conditions are cooler, drier in Utah while they are warmer, wetter in New Mexico. In Utah, sites at lower altitudes are deserts (mixture of C3 and C4) whereas sites at higher altitudes are more temperate (including deciduous and coniferous trees). Simulations were performed based on a temperate group of biomes for the highest points, and authorised desert as potential biomes for the lowest points. The New Mexico sites present higher levels of precipitation but sparser vegetation than in Utah. Simulations were performed on wooded temperate biomes for the highest site (2,438 m) and on grass biomes for the lowest sites (exclusively temperate at 2,286 m, and temperate or tropical at lower altitudes) (Table 2).

Temperature and precipitation derive from comparisons made between meteorological stations close to each elevational transect, from which temperature and precipitation lapse rates are calculated by Van de Water et al. (Δ°C by elevational meter and Δ mm year^{-1} by elevational meter). Precipitation ranges from 160 mm year^{-1} to 450 mm year^{-1} in Utah and from 360 mm year^{-1} to 610 mm year^{-1} in New Mexico. To obtain mean isotopic values, we averaged the $\delta^{13}C$ of the species balanced by the measurement number of the considered species ($\delta^{13}C$ of the whole plant derives from corrected $\delta^{13}C$ obtained on cellulose). The aim of the Van de Water et al. study was not to obtain a mean isotopic value of the landscape. The overrepresentation of some species and lack of others can bias the mean isotopic value used in our study. Mean observed $\delta^{13}C$ values range from $-23.2‰$ to $-24.8‰$ in Utah and from $-23.1‰$ to $-25.9‰$ in New Mexico.

2.5 Validation of the revised Biome4 on modern data

The calculations for the modern data are done through inverse modelling. This allows us to check at the same time the changes we incorporated in Biome4 and the inversion process. Furthermore, this provides access to uncertainty ranges, estimating of the sensitivity of the model and comparison of the model output to the field measurements.

2.5.1 Australia

The observed diversity of the vegetation community is found in the Biome4 simulation, with four biomes appearing as the most probable: Tropical Xerophytic Shrubland (TrXeShl), Tropical Evergreen Forest (TrEgFo), Warm Mixed Forest (WaMxFo), Temperate Deciduous Forest (TeDeFo) (Table 2, Fig. 1).

Except for the two lightest $\delta^{13}C$ (Glorious Mountain and Lamington, both subtropical rainforests), the simulation shows good consistency with the observation (Fig. 1a). For the two very rainy sites, a threshold effect can be observed. As water availability is not limited, $\delta^{13}C$ does not shift further. The threshold can be set at ca. 1,600 mm year^{-1} for Tropical Evergreen Forests. The relation between observed and simulated precipitation shows a greater scatter than that of $\delta^{13}C$,

Table 2 Modern data sets. This table is divided vertically into three parts (corresponding to the three geographical zone) and horizontally into four parts. The first part defines the conditions for inverse modelling with the pre-defined precipitation and temperature range for each geographical zone, the name and elevation of the different sites. The second part is devoted to vegetation: vegetation observed, potential biome groups for inverse modelling, and simulated biomes. The other parts contain parameters to be simulated ($\delta^{13}C$ and annual precipitation): on the left, observations and on the right, simulation results

	Site identification	Elevation(m)	Observed vegetation	Vegetation		Carbon isotopic composition (‰)						Observed pann	Annual precipitation (mm year^{-1})		
				Input vector: biomes field	Simulated biome	Observed $\delta^{13}C$			Simulated $\delta^{13}C$				Simulated pann		
						max	min	mean	mean	(+)	(−)		mean	(−)	(+)
Utah															
P range (−90+150%)	Ut1	2,743	Temperate	4+4: Temperate forest	TeDeFo	−20.6	−26.3	−23.8	−24.3	0.3	0.3	448	432	103	108
T range (−10+15°C)	Ut2	2,591		4+4: Temperate forest	TeDeFo	−19.0	−26.4	−23.8	−24.3	0.3	0.3	420	365	55	134
	Ut3	2.438		4+4: Temperate forest	TeDeFo	−20.7	−27.3	−24.8	−24.7	0.3	0.2	391	472	138	75
	Ut4	2,286		4+3: Temperate	TeDeFo	−20.2	−27.1	−23.9	−24.3	0.2	0.2	362	284	61	100
	Ut5	2,134		4+3: Temperate	TeGrl	−20.0	−27.2	−23.9	−24.4	0.2	0.4	333	318	82	82
	Ut6 (*)	1,981		4+3: Temperate	TeDeFo	−20.0	−27.1	−24.0	−24.5	0	0.4	304	372	48	140
	Ut7	1,829		4+3: Temperate	TeGrl	−19.3	−26.3	−23.6	−24.3	0.1	0.3	275	271	47	74
	Ut8	1,676		4+3: Temperate	TeGrl	−19.5	−25.7	−23.3	−24.2	0.2	0.3	246	280	69	76
	Ut9	1,524		3+2: Trop temp grassland	Desert	−19.3	−27.1	−23.4	−23.6	0.2	0.3	217	154	64	61
	Ut10	1,372		3+2: Trop temp grassland	Desert	−21.0	−26.2	−23.3	−23.7	0.1	0.4	188	128	51	83
	Ut11	1,219	Desert	3+2: Trop temp grassland	Desert	−21.3	−24.5	−23.2	−23.6	0.1	0.3	159	150	70	56
New Mexico															
P range (−90+300%)	Nmex 1 (*)	2,438	Temperate	3+4: Temperate	TeBlSa	−28.3	−23.7	−25.9	−26	0.3	0.3	610	564	140	47
T range (−10+15°C)	Nmex 2	2,286		3+3: Temp grassland	TeGrl	−27.7	−21.5	−23.6	−24.2	0.1	1.3	560	558	318	46
	Nmex 3	2,134		3+2: Temp trop grassland	TeXeShl	−27.9	−21.7	−24.2	−24.7	0.2	0.3	510	258	53	82
	Nmex 4	1,981		2+3: Trop temp grassland	TeGrl	−26.4	−20.4	−23.4	−24.1	0.3	1.1	459	276	74	277
	Nmex 5	1,829		2+3: Trop temp grassland	TeGrl	−25.7	−20.1	−23.2	−22.8	0.8	0.1	409	283	23	277
	Nmex 6	1,676	Grassland	2+3: Trop temp grassland	TeGrl	−25.7	−21.1	−23.1	−24.1	0	1.8	359	451	226	102
Australia															
P range (−90+300%)	Currawinya NP	200	Mulga	2+2: Tropical grassland	TrXeShl	−24.5	−29.7	−26.6	−26.5	0.3	0.2	294	338	40	451
T range (−25+15°C)	Idalia NP (*)	420	Brigalow	1+2: Tropical	TrXeShl	−22.5	−29.0	−25.6	−25.8	0.2	0.5	450	261	−6	554
	Bell/Jandowae	420	Open savannah woodland	2+2: Tropical grassland	TrXeShl	−24.9	−31.5	−28.0	−28	0.1	0.1	672	735	128	352
	Mt Berriman	400	Dry rainforest/vine thicket	1+4: Trop temp forest	WaMxFo	−26.7	−31.1	−28.9	−29	0.1	0.3	836	1,100	258	347
	Gambubal SF	1100	Subtropical rainforest	1+2: Tropical	TrXeShl	−27.1	−33.9	−30.0	−29.8	0.2	0.2	1,199	1,408	527	238
	Coominya	500	Open forest	1+4: Trop temp forest	WaMxFo	−24.8	−28.6	−27.2	−27.2	0.3	0.3	822	1,098	372	211
	Mt Glorious	640	Subtropical rainforest	1+1: Tropical forest	TrEgFo	−26.0	−34.2	−30.6	−29.8	0.2	0.2	1,687	1,506	107	191
	Pine mountain	135	Dry rainforest	1+4: Trop temp forest	WaMxFo	−23.2	−32.4	−27.3	−27.5	0	0.4	882	1,149	494	187
	Mt Coo-tha	232	Open forest	1+4: Trop temp forest	TeDeFo	−27.9	−29.4	−28.7	−28.6	0.4	0.2	1,246	1,292	442	280
	Beerwah SF	15	Wet coastal heatland	1+1: Tropical forest	TrEgFo	−27.0	−31.1	−29.3	−29.4	0.1	0.2	1,616	1,338	131	196
	Loganholme	25	Swamp	1+2: Tropical	TeXeShl	−25.0	−30.9	−28.9	−29	0.1	0.2	1,244	1,024	278	190
	Lamington NP	700	Subtropical rainforest	1+1: Tropical forest	TeEgFo	−26.8	−34.6	−31.2	−29.7	0.4	0.2	1,645	1,616	249	93

although it remains consistent in light of the uncertainties (Fig. 1b). This scatter is observed for Loganholme, Berriman Mountain, Pine Mountain and Coominya. Loganholme is characterised by the authors as a "swamp". This particular hydrological situation can be at the origin of the underestimation of the precipitation level. For Berriman Mountain, Pine Mountain and Coominya, the simulated precipitation is higher than observed and they are all simulated by a Warm Mixed Forest (WaMxFo). This overestimation can be linked to the Biome4 itself. For forests, the canopy effect is only partially taken into account. The canopy effect has two major impacts: first, a limited diffusion of CO_2 (resulting from mineralisation of soil organic matter) and consequently a higher CO_2 concentration available for plants, and secondly a decrease of the CO_2 isotopic composition. Indeed, the CO_2 resulting from the degradation of soil organic matter shows an isotopic composition of around $-25‰$, that tends to bring the δ^{13}Catm down to a more negative value than the $-7.85‰$ set in the input vector. Consequently, even if ^{13}C fractionation from atmosphere to plant remains the same, the observed isotopic signature of plants appears as more negative in closed environments than in open landscapes. Thus, as this canopy effect specificity is omitted in Biome4, the precipitation simulated for closed landscapes might be slightly overestimated, but within the uncertainty range.

2.5.2 United States

As shown in Table 2, the Utah data include biomes ranging from Temperate Deciduous Forest (TeDeFo) and TeGrl from 2,750 m to 1,830 m to Desert under 1,530 m, and are in line with observations. Likewise, the New Mexico data characterise biomes ranging from Temperate Broadleaved Savanna (TeBlSa) at the highest altitude to Temperate Grassland (TeGrl) under 2,290 m, except at 2,134 m where a Temperate Xerophytic Shrubland (TeXsShl) appears as the most probable biome (Table 2, Fig 1).

As shown in Fig. 1, the agreement between simulated results and observations is good for both δ^{13}C and precipitation. One observed δ^{13}C value from the New Mexico site at 2,134 m falls outside the general trend for New Mexico, showing values that are increasingly negative with altitude. To reach this δ^{13}C through the inversion procedure, Biome4 has to simulate a TeXeShl instead of a TeGrl, as it does for the 2,286 m and 1,981 m levels framing 2,134 m. This could explain the discrepancy between simulated and observed precipitation.

Relationships between observations and simulations from the three modern data sets are close to 1:1, with respective slopes of 0.90 ± 0.02 ($r^2 = 0.98$, $n = 29$) for δ^{13}C and 0.97 ± 0.06 ($r^2 = 0.90$, $n = 29$) for precipitation (Fig. 1). This consistency further validates the additions inserted in the original Biome4 model.

3 Application

3.1 Set of paleodata: the Nußloch loess sequence

The revised version of Biome4 is applied to a δ^{13}C record of loess organic matter in the Rhine Valley. The Nußloch loess sequence covers a great part of the last climatic cycle, but only the last 83 kyr period is considered here. The isotopic record and chronology are presented elsewhere (Hatté et al. 2001b; Lang et al. 2003) and are shown in Fig. 2a. For the isotopic study, the Nußloch sequence was sampled by taking 1–2 g sediments at intervals of 5–10 cm and by analyzing bulk carbon isotopic composition. δ^{13}C values vary from -25.72 to $-23.52 \pm 0.15‰$. Considering the low level of CO_2 concentration during glaciation, such isotopic values characterise the presence of only C3 plants all along the considered period.

Antoine et al. (2001) presented the pedostratigraphy and sedimentology. Briefly, the Nußloch loess sequence is 18 m thick. The basal soil complex underwent a pedosedimentary evolution (Luvisol/Greyzem/"steppe soil") characterising the classic progression towards increasing continentality, from the end of the Eemian to the beginning of the full glacial stage. The pedocomplex expanded by 60 cm between ca. 100 and 67 kyr BP. Pedology and palynology attest the presence of boreal forest with pine and birch. In this study, only the Greyzem and "steppe soil" are considered. Thereafter, typical loess deposited over 16 m between ca. 67 to 15 kyr BP during the Pleniglacial phase. According to the ^{14}C ages (Hatté et al. 2001b), a hiatus occurred during the 34–46 kyr period. Two Cambisols, known as Lohner Boden and Gräselberger Boden interstratified the typical loess. They are associated with a climatic improvement marked by the presence of some trees, clearly attested by pedology and malacology (Antoine et al. 2001; Moine et al. 2002). The upper levels of the sequence represent early Holocene, i.e. temperate vegetation with deciduous trees.

For most of the sequence, the input vector sets the "boreal grasslands" group of biomes (n° 6, see Fig. 2b) as the only possible one. For the Cambisols, the input vector is either "boreal grasslands" or "boreal forests" (6–5). The basal Greyzem and "steppe soil" are defined as "boreal forests" because they are associated with pine forest (Antoine et al. 2001). Finally, a succession from "boreal grasslands" (6–6) to "temperate forests" (4–4) is proposed for the upper first meter. In the soil grid provided by the Food and Agriculture Organisation (FAO), we considered a soil in northern Asia (Kirghizstan) as representative of a glacial Nußloch environment. The soil parameters of the boreal forest come from a modern soil in Northern Canada.

The isotopic composition of atmospheric CO_2 is obtained from a smoothed signal of the Leuenberger et al. (1992) original measurements, re-sampled for the last 43 kyr using the Nußloch scale and considering a con-

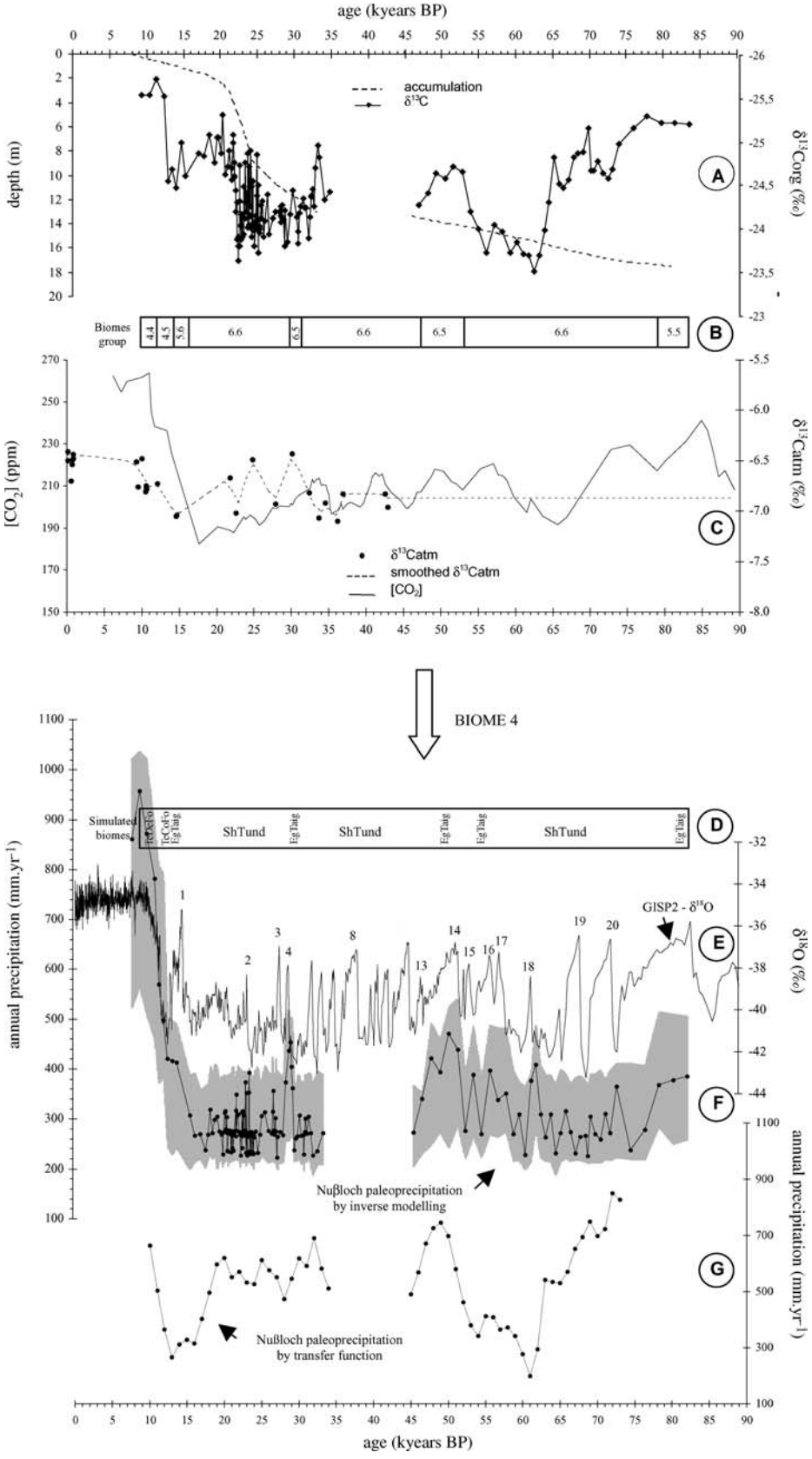

Fig. 2 Paleo data set. All the data is presented versus an age-scale in kyr cal BP. ^{14}C-ages are calibrated using Calib 4.3 (Stuiver and Reimer 1993) for the last 22 kyr and translated into calendar age using the study of Kitagawa and van Der Plicht (1998) for older periods. From top to bottom: (**a**) δ^{13}C record (*solid line*) and accumulation diagram (*dotted line*) of the Nußloch loess sequence, (**b**)biomes groups as proposed in the inverse modelling input vector, (**c**) isotopic composition (derived from Leuenberger et al. 1992) and concentration of atmospheric CO_2 (derived from Petit et al. 1999 and Indermühle et al. 2000) as introduced in the inverse modelling input vector, (**d**) simulated biomes as output of inverse modelling, (**e**) Greenland ice-core GISP2 δ^{18}O (Grootes et al. 1993; Sowers et al. 1993; Meese et al. 1994; Stuiver et al. 1995), (**f**) precipitation reconstruction obtained by inverse modelling, grey zone for global uncertainty range and circles for modal values, (**g**) paleoprecipitation reconstruction based on the transfer function (Hatté et al. 2001a)

stant value (−6.87‰) for older points (Fig. 2c). The atmospheric CO_2 record derives from Petit et al. (1999) and Indermühle et al. (2000). The first one covers completely the period of the Nußloch record, but presents a weak temporal resolution (a mean of 2500 years, from 600 years to 6,000 years, along the 15–85 kyr). The

second one was performed with a higher temporal resolution (mostly around 550 years) consistent with the temporal resolution of our isotopic record, especially for the period 20.3–24.5 kyr where a time slice between two consecutive 100-year samples is frequent. Unfortunately, this last record runs only from 20 kyr to 60 kyr. Both records being based on the GT4 chronology, we used a composite record of CO_2 concentration obtained by resampling both signals with the Nußloch time-scale (Fig. 2c).

The inverse modelling process is performed using initial sampling increments from −25°C to +15°C of modern January and July temperatures and −80 to +40% of modern January and July precipitation. The initial value of S^2, the model precision, is set at five.

3.2 Results and discussion

The outputs of inverse modelling applied to the Nußloch loess sequence are of three types: simulated biome (Fig. 2d and a zoom in Fig. 3), simulated $\delta^{13}C$ (Fig. 4) and palaeoprecipitation reconstruction (Fig. 2d). Sedimentological, malacological and geochemical studies performed on loess provide a comparison between possible biomes's and $\delta^{13}C$'s simulated and observed data. We do not consider temperatures, as they are less constrained by $\delta^{13}C$ than is the case for precipitation.

Biome4 simulates a Shrub Tundra (ShTund) along with the typical loess deposit, and sometimes shows a competition with an Evergreen Taiga (EgTaig) and/or a Cool Mixed Forest (ClMxFo) (Fig. 2d). Deglaciation follows the trend to more temperate conditions: from a ShTund to a TeDeFo, through EgTaig and Temperate Coniferous Forest (TeCoFo). The "Greyzem/steppe soil" vegetation is simulated as an EgTaig. All of these inversion results are in agreement with the pedological and malacological bio-indicators (Antoine et al. 2001; Moine et al. 2002). The two Cambisol are nevertheless simulated by closer vegetation (EgTaig) than expected, due to the absence of a modern analogue for a "very open steppe covered by 20–30% of birches" (Antoine et al. 2001). The transition from closed to open vegetation is not linked to the initial conditions defined in the input vector of the inversion procedure, but is directly related to the climatic and environmental conditions. The fine structure of the biome distribution (given by the Monte Carlo algorithm) clearly records the progressive transition from open vegetation to taiga. This is obvious for the 60–45 kyr BP period framing the development of the "Gräselberger Boden" (Fig. 3). If, before 60 kyr, the ShTund appears clearly as the most probable biome, the competition with closer vegetation comes as early as 59.5 kyr BP. This competition finally expresses an EgTaig as the most probable biome between 52 kyr and 48 kyr BP. The return to ShTund occurs as early as 47.5 kyr BP, whereas the input vector allows both five and six biomes groups, i.e. trees presence, until 47.2 kyr BP. The occurrence of open or closed vegetation is not a solution by default, but really reflects a vegetation response to climatic forcing. The precise constraint of biome groups in the input vector is only a way of narrowing the ranges of precipitation and temperature.

The $\delta^{13}C$ output ranges from −23‰ to −26.5‰ (mean uncertainty range: ±0.5‰) and is in agreement with observations ($r^2 = 0.75$, $n = 164$, Fig. 4). Nevertheless, some discrepancies may be identified, particularly during the ca. 62–58 kyr BP period, for which simulations present lower values than observations. The causes of the "$\delta^{13}C$ mismatches" between the data and the model may arise either from the Biome4 model itself or from the isotopic data:

(a) The absence of modern analogues for palaeoassemblages can be referred to, as for all paleoclimatic analyses. Biome categories are based upon present vegetation, and thus do not accommodate the possibility that vegetation units may have existed

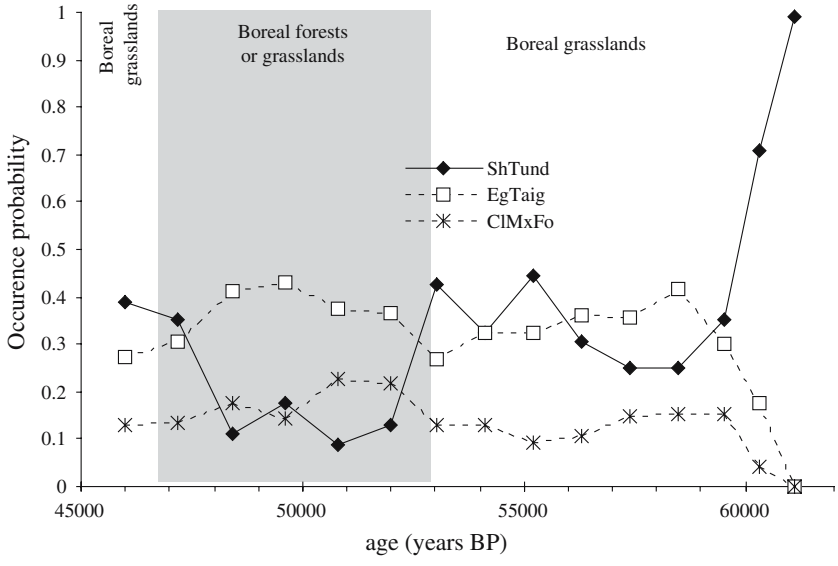

Fig. 3 Probability of occurrence for three biomes: Shrub Tundra (ShTund, *solid diamonds* and *solid line*), Evergreen Taiga (EgTaig, *open squares* and *dashed line*) and Cool Mixed Forest (ClMxFo, *stars* and *dashed line*) for the 61–45 kyr interval. The grey zone shows the period for which the input vector proposed boreal forests or grasslands, as opposed to single boreal grasslands

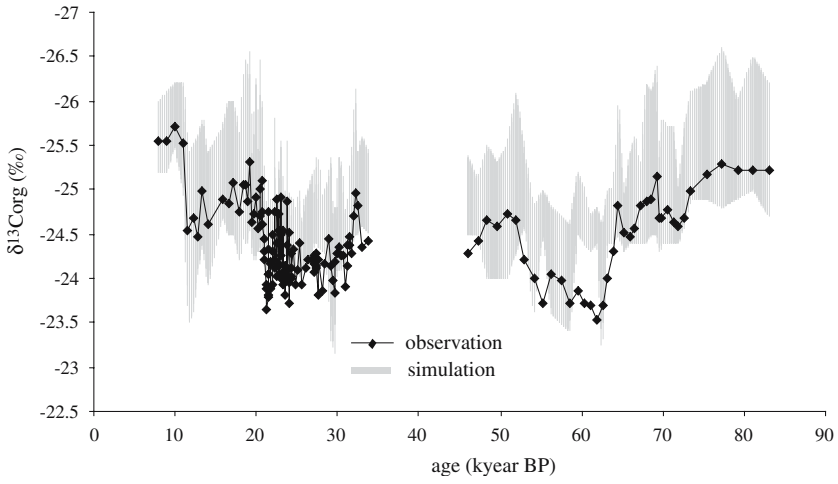

Fig. 4 observed (*solid line*) and simulated (*grey zone*) $\delta^{13}C$ versus age-scale. The correlation factor is ca. 0.75 for 164 observations

in the past under environmental conditions with no extensive modern equivalent that do not match directly any contemporary biome. As an example, the ''very open steppe covered by 20–30% of birches'', associated to Cambisol, is not easy to represent in terms of present biomes. Likewise, the specificity of loess deposit cannot be found in present soil development conditions: nowhere does such dust accumulation exist and nowhere is there a place saved by pedogenesis.

(b) The vegetation model can also be referred to. In the Biome4 model, the albedo and incoming solar radiation are set at a constant corresponding to their modern values, even though they display important fluctuations all along the last glaciation period, with repercussions on plant physiology.

(c) The discontinuous sampling performed for the isotopic study can distort the magnitude of the changes in the simulated $\delta^{13}C$. A punctual sampling of loess, 1 g each 10 cm, corresponds to a random sampling of climatic variations.

(d) The input vector of the inverse modelling includes isotopic composition of atmospheric CO_2. Due to the sparse values available, we had to assign a constant value to periods older than 43 kyr BP, even though a variability of 1–1.5‰ is observed (Eyer et al. 2004).

Besides this slight discrepancy, the general agreement between simulations and observations is good, as indicated by the r^2 value equal to 0.75. Therefore, we are founded to interpret the palaeoprecipitation reconstruction in climatic terms.

The inverse modelling simulates palaeoprecipitation ranging from 280^{+120}_{-60} mm year^{-1} to 460^{+80}_{-160} mm year^{-1} along the glaciation period (Fig. 2f), well below the modern value of about 800 mm year^{-1}. This aridity is in agreement with pedological and malacological bio-indicators (Antoine et al. 2001; Moine et al. 2002). This range is also lower than the values derived from the transfer function previously used (Fig. 2g, Hatté et al. 2001b), where an overestimation of glacial precipitation at its contemporary value was already indicated. The palaeoprecipitation reconstruction obtained by inverse modelling can be divided into three parts. Prior to 28 kyr BP, precipitation varies from 280^{+120}_{-60} mm year^{-1} to 460^{+80}_{-160} mm year^{-1} and is relatively constant in the ca. 28−15 kyr BP range. It finally increases during deglaciation.

The period before 28 kyr BP shows large oscillations of about 150–200 mm year^{-1}. These are very similar and contemporaneous to some Dansgaard-Oeschger events (D/O) as recorded by Greenland ice-cores (GISP2 $\delta^{18}O$, Grootes et al. 1993; Sowers et al. 1993; Meese et al. 1994; Stuiver et al. 1995). The D/O 14, 15, 16, 18 as well as three or four are particularly well recognisable (Fig. 2e, f). The D/O 14, that is associated with a temperature shift of 10–12°C in Greenland (derived from Dahl-Jensen et al. 1998; Lang et al. 1999; Landais et al. 2004), is marked by a precipitation increase of 200 mm year^{-1}, i.e. +ca. 70%. The very similar and contemporaneous signals in both the Greenland and Nußloch do not represent an artefact, due to the variability of the global signals. This is particularly clear prior to 43 kyr BP when the $\delta^{13}C$atm values are stable, whereas when they vary after 43 kyr BP, they are not in phase with the fluctuations of palaeoprecipitation, especially with respect to D/O 3–4. In addition, the maxima of the precipitation systematically lead those of CO_2 concentration. Furthermore, the CO_2 variations are ca. 20 ppm. According to Feng and Epstein (1995), this would be reflected by a $\delta^{13}C$ shift of about 0.4‰ and thus explain a change of precipitation of only 60 mm year^{-1}. The similarity expressed in both GISP2 and Nußloch evidences a close link between precipitation regime, polar and continental ice-sheets size, sea level and consequently polar front position. At the first order, $\delta^{18}O$ changes in ice are linked to those of the atmospheric temperature and depend on the ice-sheet size: the smaller the ice-sheet, the more positive is the $\delta^{18}O$ and the higher the temperature. This pulls the polar front to the North Atlantic high latitudes, favouring a

mild oceanic regime over Western Europe and over the Nußloch site. Alternatively, during stadials the polar front moved southwards (Ruddiman and McIntyre 1981), limiting the inflow of wet air over Europe.

A nearly constant level of precipitation at around 280 mm year^{-1} is observed between 28 kyr and 17 kyr BP during full glacial conditions (Fig. 2f). At that time, the English Channel had mostly emerged (sea-level ca. 90 m below present conditions, Waelbroeck et al. 2002). Such a geographical configuration is consistent with a great reduction of the inflow of wet oceanic air fluxes. Nußloch is thus less sensitive to changes in the polar front position during that time interval.

The deglaciation and Holocene onset are characterised by higher precipitation, reaching 960^{+80}_{-390} mm year^{-1} at ca. 9,000 years BP and decreasing to 860^{+160}_{-340} mm year^{-1} around 8,000 years BP, which is in line with the present 800 mm year^{-1} (Fig. 2f). The steady increase of precipitation associated with the deglaciation is interrupted by a step between 14 kyr and 12.5 kyr BP, which one is tempted to relate to the Younger Dryas.

These precipitation results show a picture consistent with the malacological and pedological analyses of the loess sequence, as well as with the climatic conditions over both the oceanic and the cryospheric areas. The use of vegetation models clearly provides the expected alternative to the transfer function for palaeoprecipitation reconstruction purposes.

4 Conclusion

We presented here a palaeoprecipitation record of the Nußloch sequence by using a modified version of Biome4. The inverse modelling outputs show an agreement between simulated biomes and pedological and malacological observations. Likewise, observed and simulated δ^{13}C are clearly in agreement, as indicated by the r^2 value equal to 0.75. The palaeoprecipitation reconstruction shows mean annual values from 240 mm year^{-1} to 400 mm year^{-1} during the last glaciation, well below the modern value of around 800 mm year^{-1}. It shows large fluctuations of ca. 100–200 mm year^{-1} that may be related to the Dansgaard-Oeschger events. However, this reconstruction could certainly be improved by adding constraints to the input vector used for inverse modelling, such as annual distribution of precipitation and temperature or variable insolation and albedo in the biome determination process. In the Biome4 itself, a better account of the canopy effect in the δ^{13}C calculation and of soil specificities (so as to achieve a realistic hydrological model) will improve the reconstructions. Similarly, a better knowledge of the atmospheric CO_2 signature (finer resolution of the concentration record for the whole 0–100 kyr period and advances in measurement technology for δ^{13}Catm) will increase the accuracy of the method.

The loess belts cover ca. 10% of the emerged surface (Pécsi 1990). Inverse modelling based on organic geochemistry in loess opens an opportunity to better understand, reconstruct and simulate past hydrology, and to map a general pattern of atmospheric circulation by reconstructing precipitation changes during glacials.

Acknowledgements This research was funded by the French INSU/CNRS "Programme National d'Étude de la Dynamique du Climat" VAGALAM, the CNRS, the CEA and by the European Union 5th PCRD (project MOTIF EVK2-2001-00263). The Nußloch fieldwork was possible thanks to the permission of Heidelberger Zement AG and was supported by the EC Program (BIMACEL) and the French ECLIPSE program (EOLE and EOLE2). We are especially grateful to Denis-Didier Rousseau and Pierre Antoine, leaders of these programs, for their help and discussions. We would like to thank P. Van de Water and G. Stewart for providing original data and J. Kaplan for providing the Biome4 model source code. Valuable comments from Andrew Friend, Evelyn Cottereau, Philip Meyer, Martine Paterne, Colin Prenctice and two anonymous reviewers helped to greatly improve the manuscript. This is LSCE-contribution n°1238.

References

Antoine P, Rousseau DD, Zöller L, Lang A, Munaut A-V, Hatté C, Fontugne MR (2001) High-resolution of the last interglacial-glacial cycle in the loess paleosol sequences of Nussloch (Upper Rhine Area, Germany). Quaternary Int 76/77:211–229

Bond GC, Broecker W, Johnsen S, McManus J, Labeyrie LD, Jouzel J, Bonani G (1993) Correlations between climate records from North-Atlanic sediments and Greenland ice. Nature 365:143–147

Boom A, Marchant R, Hooghiemstra H, Sinninghe Damsté JS (2002) CO_2- and temperature-controlled altitudinal shifts of C4- and C3-dominated grasslands allow reconstruction of palaeoatmospheric pCO_2. Palaeogeogr Palaeoclimatol Palaeoecol 177:151–168

Constable GA, Rawson HM (1980) Effect of leaf position, expansion and age on photosynthesis, transpiration and water use efficiency of cotton. Aust J Plant Physiol 7:89–100

Dahl-Jensen D, Mosegaard K, Gunderstrup GD, Clow GD, Johnsen SJ, Hansen AW, Balling N (1998) Past temperatures directly from the Greenland ice sheet. Science 282:268–271

Dansgaard W, Johnsen SJ, Clausen HB, Dahl-Jensen NS, Gundestrup NS, Hammer CU, Hvidberg CS, Steffensen JP, Sveinbjörnsdottir AE, Jouzel J, Bond GC (1993) Evidence for general instability of past climate from a 250-ky ice-core record. Nature 364:218–220

Duranceau M, Ghashghaie J, Badeck F, Deleens E, Cornic G (1999) δ^{13}C of CO_2 respired in the dark in relation to δ^{13}C of leaf carbohydrates in *Phaseolus vulgaris* L. under progressive drought. Plant Cell Environ 22:515–523

Eyer M, Leuenberger M, Nyfeler P, Stocker TF (2004) Comparison of two $\delta^{13}CO_2$ records measured on air from the EPICA Dome C and Kohnen Station ice cores. European Geosciences Union, 1st General Assembly, EGU04-A-01990

Farquhar GD, O'Leary MH, Berry JA (1982) On the relationship between carbon isotope discrimination and the intercellular carbon dioxide concentration in leaves. Aust J Plant Physiol 9:121–137

Feng X, Epstein S (1995) Carbon isotopes of trees from arid environments and implications for reconstructing atmospheric CO_2 concentration. Geochimica et Cosmochimica Acta 59:2599–2608

Francey RJ, Gifford RM, Sharkey TD, Weir B (1985) Physiological influences on carbon isotope discrimination in huon pine (*Lagarostrobos franklinii*). Oecologia 66:211–218

Genty D, Blamart D, Ouahdi R, Gilmour M, Baker A, Jouzel J, Van ES (2003) Precise dating of Dansgaard-Oeschger climate oscillations in western Europe from stalagmite data. Nature 421(6925):833–837

Grimm EC, Jacobson GL, Watts WA, Hansen BCS, Maasch KA (1993) A 50,000-year record of climate oscillations from Florida and its temporal correlation with the Heinrich events. Science 261:198–200

Grootes PM, Stuiver M, White JWC, Johnsen S, Jouzel J (1993) Comparison of oxygen isotope records from the GISP2 and GRIP Greenland ice cores. Nature 366:552–554

Guiot J, Torre F, Jolly D, Peyron O, Boreux JJ, Cheddadi R (2000) Inverse vegetation modeling by Monte Carlo sampling to reconstruct palaeoclimates under changed precipitation seasonality and CO_2 conditions: application to glacial climate in Mediterranean region. Ecol Model 127:119–140

Guo Z, Liu T, Guiot J, Wu N, Han J, Liu J, Gu Z (1996) High frequency pulses of East Asian monsoon climate in the two glaciations: link with the North Atlantic. Clim Dynam 12:701–709

Hastings WK (1970) Monte-Carlo sampling methods using Markov chains and their application. Biometrika 57:97–109

Hatté C, Fontugne MR, Rousseau D-D, Antoine P, Tisnérat-Laborde N (1998) $\delta^{13}C$ variations of loess organic matter as a record of the vegetation response to climatic changes during the Weichselian. Geology 26:583–586

Hatté C, Antoine P, Fontugne MR, Rousseau D-D, Tisnérat-Laborde N, Zöller L (1999) New chronology and organic matter $\delta^{13}C$ paleoclimatic significance of Nußloch loess sequence (Rhine Valley, Germany). Quaternary Int 62(1):85–91

Hatté C, Antoine P, Fontugne MR, Lang A, Rousseau D-D, Zöller L (2001a) $\delta^{13}C$ variation of loess organic matter as a potential proxy for paleoprecipitation. Quaternary Res 55:33–38

Hatté C, Pessenda LCR, Lang A, Paterne M (2001b) Development of an accurate and reliable ^{14}C chronology for loess sequences. Application to the loess sequence of Nußloch (Rhine valley, Germany). Radiocarbon 43(2B):611–618

Haxeltine A, Prentice IC (1996) BIOME 3: an equilibrium terrestrial biosphere model based on ecophysiological constraints, resource availability and competition among plant functional types. Global Biogeochem Cy 10(4):693–709

Hsu JC, Smith BN (1972) ^{13}C ratios of carbon dioxide from peanut and sunflower seedlings and tobacco leaves in light and in darkness. Plant Cell Physiol 13:689–694

Indermühle A, Monnin E, Stauffer B, Stocker TF, Wahlen M (2000) Atmospheric CO_2 concentration from 60 to 20 kyr BP from the Taylor Dome ice core, Antarctica. Geophys Res Lett 27(5):735–738

Kaplan JO, Prentice IC, Buchmann N (2002) The stable carbon isotope composition of the terrestrial biosphere: modeling at scales from the leaf to the globe. Global Biogeochem Cycle 16(4):1060, doi:10.1029/2001GB001403

Kitagawa H, van der Plicht J (1998) Atmospheric radiocarbon calibration to 45,000 yr B.P.: late glacial fluctuations and cosmogenic isotope production. Science 279:1187–1190

Krishnamurthy RV, Epstein S (1990) Glacial-interglacial excursion in the concentration of atmospheric CO_2: effect in the $^{13}C/^{13}C$ ratio in wood cellulose. Tellus 42B:423–434

Landais A, Caillon N, Goujon C, Grachev A, Barnola J-M, Chappellaz J, Jouzel J, Masson-Delmotte V, Leuenberger M (2004) Quantification of rapid temperature change during DO event 12 and phasing with methane inferred from air isotopic measurements. Earth Planet Sc Lett 225:221–232

Lang A, Hatté C, Rousseau D-D, Antoine P, Fontugne MR, Zöller L, Hambach U (2003) High-resolution chronologies for loess: comparing AMS ^{14}C and optical dating results. Quaternary Sci Rev 22:953–959

Lang C, Leuenberger M, Schwander J, Johnsen SJ (1999) 16°C rapid temperature variation in central Greenland 70,000 years ago. Science 286:934–937

Leuenberger M, Siegenthaler U, Langway CC (1992) Carbon isotope composition of atmospheric CO_2 during the last ice age from an Antarctica ice core. Nature 357:488–490

Lin G, Ehleringer JR (1997) Carbon isotopic fractionation does not occur during dark respiration in C3 and C4 plants. Plant Physiol 114:391–394

Lloyd J, Farquhar GD (1994) ^{13}C discrimination during CO_2 assimilation by the terrestrial biosphere. Oecologia 99:201–215

Meese D, Alley RB, Gow T, Grootes PM, Mayewski PA, Ram M, Taylor KC, Waddington E, Zielinski G (1994) Preliminary depth-age scale of the GISP2 ice core. Cold Region Research and Engineering Laboratory

Moine O, Rousseau D-D, Antoine P, Hatté C (2002) Mise en évidence d'évènements climatiques rapides par les faunes de mollusques terrestres des loess Weichséliens de Nussloch (Allemagne). Quaternaire 13(3/4):209–217

Park R, Epstein S (1961) Metabolic fractionation of ^{13}C and ^{13}C in plants. Plant Physiol 36:133–138

Pasquier-Cardin A, Allard P, Ferreira T, Hatté C, Coutinho R, Fontugne MR, Jaudon M (1999) Magma-derived CO_2 emissions recorded in ^{14}C and ^{13}C content of plants growing in Furnas Caldera, Azores. J Volcanol Geother Res 92:195–207

Pécsi M (1990) Loess is not just the accumulation of dust. Quaternary Int 7/8:1–21

Petit JR, Jouzel J, Raynaud D, Barkov NI, Barnola JM, Basile I, Bender M, Chappellaz J, Davis M, Delaygue G, Delmotte M, Kotlyakov VM, Legrand M, Lipenkov V, Lorius C, Pépin L, Ritz C, Saltzman E, Stievenard M (1999) Climate and atmospheric history of the past 420,000 years from the Vostok ice core, Antarctica. Nature 399:429–436

Porter SC, Zhisheng A (1995) Correlation between climate events in the north Atlantic and China during the last glaciation. Nature 375:305–308

Rousseau D-D (1991) Climatic transfer function from quaternary molluscs in European loess deposits. Quaternary Res 36:195–209

Rousseau D-D, Antoine P, Hatté C, Lang A, Zöller L, Fontugne MR, Ben Othman D, Luck J-M, Moine O, Labonne M, Bentaleb I, Jolly D (2002) Abrupt millenial climatic changes from Western European eolian records during the last glaciation. Quaternary Sci Rev 21:1577–1582

Ruddiman W, McIntyre A (1981) The North-Atlantic ocean during the last deglaciation. Palaeogeogr Palaeoclimatol Palaeoecol 35(2–4):145–214

Scholze M, Kaplan JO, Knorr W, Heimann M (2003) Climate and interannual variability of the atmosphere-biosphere. Geophys Res Lett 30(2):69–1, 69–4

Sharkey TD, Raschke K (1981) Separation and measurement of direct and indirect effects of light on stomata. Plant Physiol 68:33–40

Sowers T, Bender M, Labeyrie LD, Martinson D, Jouzel J, Raynaud D, Pichon J-J, Korotkevich Y (1993) 135,000 year Vostok-SPECMAP common temporal framework. Palaeogeogr Palaeoclimatol Palaeoecol 8:737–766

Stewart GR, Turnbull MH, Schmidt S, Reskine PD (1995) ^{13}C natural abundance in plant communities along a rainfall gradient: a biological integrator of water availability. Aust J Plant Physiol 22:51–55

Stuiver M, Grootes PM, Braziunas TF (1995) The GISP2 $\delta^{18}O$ climate record of the past 16,500 years and the role of the sun, ocean, and volcanoes. Quaternary Res 44:341–354

Stuiver M, Reimer PJ (1993) Extended ^{14}C data base and revised calib 3.0 ^{14}C age calibration program. Radiocarbon 35(1):215–230

Troughton JH, Card KA, Hendy CH (1974) Photosynthetic pathways and carbon isotope discrimination by plants. Carnegie Inst Wash Yearbook 73:768–780

Van de Water PK, Leavitt SW, Betancourt JL (1994) Trends in stomatal density and $^{13}C/^{13}C$ ratios of *Pinus flexilis* needles during last glacial-interglacial cycle. Science 264:239–243

Van de Water PK, Leavitt SW, Betancourt JL (2002) Leaf $\delta^{13}C$ variability with elevation, slope aspect, and precipitation in the southwest United States. Oecologia 132:332–343

Waelbroeck C, Labeyrie LD, Michel E, Duplessy J-C, McManus J, Lambeck K, Balbon E, Labracherie M (2002) Sea-level and deep-water temperature changes derived from benthic foraminifera isotopic records. Quaternary Sci Rev 21:295–305

Wong WW, Benedict CR, Kohel RJ (1979) Enzymatic fractionation of the stable carbon isotopes of carbon dioxide by ribulose-1,5-biphosphate carboxylase. Plant Physiol 63:852–856